Am J Physiol Lung Cell Mol Physiol 295: L552–L565, 2008.
First published July 25, 2008; doi:10.1152/ajplung.90287.2008.

Inhalation vs. aspiration of single-walled carbon nanotubes in C57BL/6 mice: inflammation, fibrosis, oxidative stress, and mutagenesis

A. A. Shvedova,[1,3] E. Kisin,[1] A. R. Murray,[1] V. J. Johnson,[2] O. Gorelik,[4,5] S. Arepalli,[4,5] A. F. Hubbs,[1] R. R. Mercer,[1,3] P. Keohavong,[8] N. Sussman,[8] J. Jin,[8] J. Yin,[8] S. Stone,[1] B. T. Chen,[1] G. Deye,[6] A. Maynard,[7] V. Castranova,[1,3,8] P. A. Baron,[6] and V. E. Kagan[8]

[1]*Pathology and Physiology Research Branch and* [2]*Toxicology and Molecular Biology Branch, Health Effects Laboratory Division, National Institute for Occupational Safety and Health (NIOSH), and* [3]*Physiology and Pharmacology, West Virginia University, Morgantown, West Virginia;* [4]*Lockheed Martin, Engineering Directorate, Materials and Processes Branch, and* [5]*Nanotube Team, GB Tech, National Aeronautics and Space Administration Johnson Space Center, Houston, Texas;* [6]*Monitoring Research and Statistical Activity, Division of Applied Research and Technology, NIOSH, Cincinnati, Ohio;* [7]*Woodrow Wilson International Center for Scholars, Washington, District of Columbia; and* [8]*Department of Environmental and Occupational Health, University of Pittsburgh, Pittsburgh, Pennsylvania*

Submitted 23 April 2008; accepted in final form 18 July 2008

Shvedova AA, Kisin E, Murray AR, Johnson VJ, Gorelik O, Arepalli S, Hubbs AF, Mercer RR, Keohavong P, Sussman N, Jin J, Yin J, Stone S, Chen BT, Deye G, Maynard A, Castranova V, Baron PA, Kagan VE. Inhalation vs. aspiration of single-walled carbon nanotubes in C57BL/6 mice: inflammation, fibrosis, oxidative stress, and mutagenesis. *Am J Physiol Lung Cell Mol Physiol* 295: L552–L565, 2008. First published July 25, 2008; doi:10.1152/ajplung.90287.2008.—Nanomaterials are frontier technological products used in different manufactured goods. Because of their unique physicochemical, electrical, mechanical, and thermal properties, single-walled carbon nanotubes (SWCNT) are finding numerous applications in electronics, aerospace devices, computers, and chemical, polymer, and pharmaceutical industries. SWCNT are relatively recently discovered members of the carbon allotropes that are similar in structure to fullerenes and graphite. Previously, we (47) have reported that pharyngeal aspiration of purified SWCNT by C57BL/6 mice caused dose-dependent granulomatous pneumonia, oxidative stress, acute inflammatory/cytokine responses, fibrosis, and decrease in pulmonary function. To avoid potential artifactual effects due to instillation/agglomeration associated with SWCNT, we conducted inhalation exposures using stable and uniform SWCNT dispersions obtained by a newly developed aerosolization technique (2). The inhalation of nonpurified SWCNT (iron content of 17.7% by weight) at 5 mg/m^3, 5 h/day for 4 days was compared with pharyngeal aspiration of varying doses (5–20 μg per mouse) of the same SWCNT. The chain of pathological events in both exposure routes was realized through synergized interactions of early inflammatory response and oxidative stress culminating in the development of multifocal granulomatous pneumonia and interstitial fibrosis. SWCNT inhalation was more effective than aspiration in causing inflammatory response, oxidative stress, collagen deposition, and fibrosis as well as mutations of K-*ras* gene locus in the lung of C57BL/6 mice.

nanoparticles; lung disease

SEVERAL DECADES OF EXTENSIVE studies of particles and their effects on the lung have revealed important mechanisms of their toxicity associated with inflammation and oxidative stress (11, 14, 38, 41, 52). The size and surface area of particles were found to be especially important as determinants of the magnitude of pulmonary responses as exemplified by augmented toxicity of microparticles, especially PM_5 and $PM_{2.5}$ (40). With the recent advent of nanotechnology, concerns have arisen that the extremely small size (<100 nm in diameter) and remarkably large specific surface area of nanoparticles may present extreme risk to human health and the environment (31, 39). Moreover, because nano-dimensions often render the chemical and physical properties of nanometer scale particles fundamentally different from larger particles of the same composition, biological and toxicological effects of nanoparticles cannot necessarily be deduced by extrapolation of data collected with fine and ultrafine particles (27). These general considerations hold true for carbon nanotubes, particularly single-walled carbon nanotubes (SWCNT), cylinders (1–3 nm in diameter) made of a single layer of graphene with lengths on the order of tens of nanometers to micrometers. A commonly used technology in the manufacturing of SWCNT is catalytic disproportionation of gaseous carbon molecules supported on catalytic iron particles. Thus raw SWCNT usually contain significant amounts (up to 40% wt) of iron that may act as a catalyst of oxidative stress. So, iron-containing SWCNT are likely more toxic than iron-free SWCNT.

Several studies have demonstrated the toxicity of SWCNT to different types of cells in vitro (7, 19, 29). However, studies of in vivo effects of SWCNT are still scarce (28, 47, 55). At the time of writing, only a few published reports demonstrate the pulmonary toxicity of SWCNT (28, 32, 47, 55). Our previous work (47) documented an unusual inflammatory response to SWCNT delivered to the lung via pharyngeal aspiration characterized by a brisk acute phase inflammatory response followed by an early onset of lung fibrosis. Inflammation and pulmonary fibrosis have been associated with an increased risk for lung cancer (20) thus justifying assessments of genotoxic events possibly accompanying SWCNT exposure.

As pharyngeal aspiration delivers SWCNT as a bolus to the lung airways, this pulmonary response could potentially be caused by the high single dose of carbon nanotubes. Recent reviews have emphasized the lack of definitive inhalation

Address for reprint requests and other correspondence: A. A. Shvedova, Health Effects Laboratory Div., NIOSH, Morgantown, WV 26505 (e-mail: ats1@cdc.gov).

The costs of publication of this article were defrayed in part by the payment of page charges. The article must therefore be hereby marked "*advertisement*" in accordance with 18 U.S.C. Section 1734 solely to indicate this fact.

studies that would avoid the potential for artifactual effects of large mats and agglomerates formed during instillation exposure procedures (10). Therefore, we developed an inhalation protocol to evaluate SWCNT effects on the lung. Because of the high propensity of hydrophobic SWCNT to agglomerate (3, 4), preparation of an adequate aerosol dispersion suitable for an inhalation protocol is immensely difficult. By applying a new technique to aerosolize SWCNT (2), we were able to obtain stable and uniform SWCNT dispersions suitable for the inhalation experiments. Here, we present the results of a study in which inhalation of nonpurified SWCNT (with an iron content of 17.7% wt) was compared with pharyngeal aspiration of various doses of the same SWCNT. We report that the inhalation route was more effective in causing inflammatory response, oxidative stress, collagen deposition, and fibrosis as well as mutations of K-*ras* gene locus in the lung of C57BL/6 mice compared with aspiration of a similar dose of SWCNT.

MATERIALS AND METHODS

Animals. Specific pathogen-free adult female C57BL/6 mice (8–10 wk) were supplied by The Jackson Laboratory (Bar Harbor, ME) and weighed 20.0 ± 1.9 g when used. Animals were housed one mouse per cage receiving HEPA filtered air in Association for Assessment and Accreditation of Laboratory Animal Care-approved National Institute for Occupational Safety and Health (NIOSH) animal facilities. All animals were acclimated in the animal facility under controlled temperature and humidity for 1 wk before use. Animals were supplied with water and certified chow 5020 (Purina Mills, Richmond, IN) ad libitum in accordance with guidelines and policy set forth by the Institute of Laboratory Animals Resources, National Research Council. All experimental procedures were conducted in accordance with a protocol approved by the NIOSH Institutional Animal Care and Use Committee.

Experimental design. Experimental protocols for the present studies included inhalation and pharyngeal aspiration exposures of C57BL/6 mice to SWCNT. Animals were exposed in a whole body inhalation exposure chambers with individual steel mesh compartments for 4 consecutive days, 5 h/day. Aerosolized SWCNT were sampled from the breathing zone within each chamber for characterization during exposure. Mice from the control group were exposed to filtered air. After the last exposure, animals were removed from the chambers and euthanized 1, 7, and 28 days postinhalation. A suspension of SWCNT (0, 5, 10, and 20 μg per mouse) was used for single pharyngeal aspiration to additional groups of C57BL/6 mice, whereas the corresponding control mice were administered sterile Ca^{2+} + Mg^{2+}-free PBS vehicle. Dose-dependent inflammatory response and pulmonary toxicity were evaluated, and the concentration of 10 μg per mouse of SWCNT was chosen for time course study. Mice were euthanized on *days 1*, *7*, and *28* following the exposure. All experiments were repeated three times. Inflammation was evaluated by total cell counts, cell differentials, and accumulation of cytokines in the bronchoalveolar lavage (BAL) fluid. Pulmonary toxicity was assessed by elevation of lactate dehydrogenase (LDH) level in acellular BAL fluid. Fibrogenic responses to exposed materials were assessed by morphometric measurements and collagen deposition. Respiratory changes after SWCNT exposures were assessed by measurement of breathing patterns using whole body plethysmography (47).

Particles. SWCNT were purchased from Carbon Nanotechnology (CNI, Houston, TX). The nanotubes were manufactured using the high-pressure CO disproportionation process (HiPco) and were used in the inhalation and pharyngeal aspiration studies as produced; i.e., without being purified or otherwise treated after the initial production process. They were supplied as a very low density dry powder. The supplied SWCNT contained nanometer-scale Fe catalyst particles inherent in the HiPco process. The amount of metallic impurities was analyzed using nitric acid dissolution and inductively coupled plasma-atomic emission spectrometry (ICP-AES) performed according to the NMAM method 7300 for trace metals (NIOSH Manual of Analytical Methods, 2005). Analysis indicates that these SWCNT contained elemental carbon (82% wt), Fe (17.7%). Trace elements present included Cu (0.16%), Cr (0.049%), and Ni (0.046%). Raman spectroscopy, near-infrared spectroscopy, and thermo-gravimetric analysis (TGA) were used for purity assessment of HiPco SWCNT. The spectra of SWCNT sample revealed distinct peaks at Raman shift of 1,586–1,591 cm^{-1}, corresponding to the characteristic G of SWCNT as well as D and G^1 bands typically found in SWCNT spectra. The diameter of SWCNT measured by transmission electron microscopy (TEM) was 0.8–1.2 nm. The length of SWCNT was 100–1,000 nm measured by Carbon Nanotechnology using atomic force microscopy. The surface area of SWCNT measured by the nitrogen absorption-desorption technique (Brunauer-Emmett-Teller method, BET) was 508 m^2/g. For pharyngeal aspiration, the suspension of SWCNT (0.7% PBS) was ultrasonicated (30 s × 3 cycles) using a Vibra-Cell High Intensity Ultrasonic Liquid Processor VCX 130 (Sonics & Materials, Newtown, CT) to improve dispersion of the particles before animal dosing.

Generation of an aerosol of SWCNT. The generation system used to deliver respirable SWCNT structures (5 mg/m^3) at a flow rate of 10 l/min to 2 animal exposure chambers each containing 12 mice as previously described (2). Briefly, aerosols containing SWCNT particles were generated using an aerosol dispersion system containing a powder feeder and a knife mill. The acoustically fluidized powder feeder, designed specifically for delivering the low-density material, allowed relatively constant feed rates over a period of ~6 h. Because the material tends to form clumps and is difficult to handle, a static discharger containing ^{210}Po strips was used to reduce the electrical charges on the particles to prevent agglomerate formation due to contact charging. In addition, a knife mill was set up to provide high shear forces to tear apart these agglomerates once they were formed. Before entering the inhalation chamber, the aerosol was passed through a settling chamber, followed by an air cyclone (GK 2.69; BGI, Waltham, MA) to remove the coarse portion of the particles from the aerosol by gravitational settling and centrifugal force. The cyclone had a 50% cutoff size of 4-μm aerodynamic diameter. The feed rate, mill speed, and air flow rate were adjusted to allow a target mass concentration of 5.0 mg/m^3 in the chamber, 5 h/day for 4 days. The mean flow rate through each animal chamber was 5 l/min.

Mass concentration. SWCNT concentration within the exposure chambers was monitored in real-time by a DataRAM (Thermo Fisher Scientific, Waltham, MA). Gravimetric samples were also taken every 30 min at 2 sites within each exposure chamber using 25-mm polyvinyl chloride (PVC) filters at a flow rate of 1 l/min.

Particle size distribution. Particle size distribution was determined by using a Micro-Orifice Uniform Deposit Impactor (MOUDI, model 110; MSP, Shoreview, MN). The flow rate of the impactor was adjusted to 30 l/min to provide the size-classified samples with the known cutoff sizes of 18-, 10-, 5.6-, 3.2-, 1.8-, 1.0-, 0.56-, 0.32-, 0.18-, 0.10-, and 0.056-μm aerodynamic diameter, respectively. PVC filters were used as the collection substrates. Oleic acid was applied to the filters (oil-soaked filters) on alternate stages to avoid the potential particle bounce and reentrainment. Separate MOUDI runs with each stage oil-soaked were analyzed for iron content by ICP-AES according to NMAM method 7300 to determine mass mode aerodynamic diameter, assuming that iron was uniformly distributed throughout the SWCNT aerosol.

Particle morphology. Particle morphology was investigated from the size-classified samples using MOUDI. Although oleic acid was required to avoid particle bounce on the collection substrate, there is a concern that the presence of oleic acid on the substrate would interfere with microscopic observations of particles. With this concern, two types of substrates were prepared, the oil-soaked PVC filters

(to prevent bounce) (Pall, Ann Arbor, MI) and the polycarbonate filters (to collect SWCNT samples) (Whatman, West Chester, PA) without any oleic acid coating. For each run, these two different substrates were placed on alternate MOUDI stages so that reliable samples (not oil-soaked) without particle loss from upper stages were obtained. By altering the stages for PVC and polycarbonate filters, a complete set of 11 samples were obtained in two runs. The mass concentration in the chamber was maintained constant during these two runs. The sample filters (polycarbonate) were prepared by applying a thin coating of Au/Pd layer for scanning electron microscopy (SEM) and attaching a 3-mm carbon-coated microscope grid at the center of the filter for TEM. This procedure was adopted because it has been successfully used in our laboratory for collecting other ultrafine particles, such as welding fume and ultrafine titanium dioxide particles.

Electron microscopy. The polycarbonate filters containing the samples of SWCNT particles were cut into equal sections and mounted onto aluminum stubs with silver paste. The deposited particles were viewed using a SEM (model 6400; JEOL, Tokyo, Japan) and also analyzed using energy dispersive X-ray analysis (SEM-EDS; Princeton Gamma Tech, Rocky Hill, NJ) at an electron beam voltage of 20 kV. Samples collected for TEM analysis were analyzed using a JEOL 1220 transmission electron microscope operating at 80 kV.

Particulate instillation. Mouse pharyngeal aspiration was used for particulate administration (43). Briefly, after anesthetization with a mixture of ketamine and xylazine (62.5 and 2.5 mg/kg subcutaneous in the abdominal area), a suspension (~50 μl) of SWCNT prepared in PBS (5, 10, and 20 μg per mouse) was placed posterior on the throat and the tongue, which was held until the suspension was aspirated into the lungs. Control mice were administered sterile Ca^{2+} + Mg^{2+}-free PBS vehicle. The mice revived unassisted after approximately 30 to 40 min. All mice in SWCNT and PBS groups survived this exposure procedure. This technique provided good distribution of particles widely disseminated in a peribronchiolar pattern within the alveolar region as was detected by histopathology. Animals treated with the particulates or PBS recovered easily after anesthesia with no behavioral or negative health outcomes. Mice were euthanized on *days 1*, *7*, and *28* following the exposures.

Obtaining BAL from mice. Mice were euthanized with intraperitoneal injection of sodium pentobarbital (>100 mg/kg) and exsanguinated. The trachea was cannulated with a blunted 22-gauge needle, and BAL was performed using cold sterile PBS at a volume of 0.9 ml for first lavage (kept separate) and 1.0 ml for subsequent lavages. Approximately 5 ml of BAL fluid per mouse was collected in sterile centrifuge tubes. Pooled BAL cells for each individual mouse were washed in PBS by alternate centrifugation (800 *g*, 10 min, 4°C) and resuspension. Cell-free first fraction BAL aliquots were stored at 4°C for LDH assays, and the remainder was frozen at −80°C until processed.

BAL cell counting and differentials. The degree of inflammatory response was estimated by quantitating total cells, macrophages, and polymorphonuclear leukocytes (PMNs) recovered by BAL. Cell counts were performed using an electronic cell counter equipped with a cell-sizing attachment (Coulter Multisizer II with a 256C channelizer; Coulter Electronics, Hialeah, FL). Alveolar macrophages (AM) and PMNs were identified by their characteristic cell shape in cytospin preparations stained with Diff-Quick (Fisher Scientific, Pittsburgh, PA), and differential counts of BAL cells was carried out. Three hundred cells per slide were counted.

Lung lavage fluid cytokine analysis. Levels of cytokines were assayed in the acellular BAL fluid following SWCNT inhalation or aspiration exposures. The concentrations of TNF-α and IL-6 (sensitivity of assay is 5–7.3 pg/ml) were determined using the BD Cytometric Bead Array Mouse Inflammation Kit (BD Biosciences, San Diego, CA). The concentrations of active transforming growth factor-β1 (TGF-β1) (sensitivity of assay is <15.6 pg/ml) was determined using an ELISA kit (BioSource International, Camarillo, CA).

Total protein and LDH activity in the BAL fluid. Measurement of total protein in the BAL fluid was performed by a modified Bradford assay according to the manufacturer's instructions (Bio-Rad, Hercules, CA) with BSA as a standard. The activity of LDH was assayed spectrophotometrically by monitoring the reduction of nicotinamide adenine dinucleotide at 340 nm in the presence of lactate using Lactate Dehydrogenase Reagent Set (Pointe Scientific, Lincoln Park, MI).

Lung preparation for microscopic evaluation. Preservation of the lung was achieved by vascular perfusion of a glutaraldehyde (2%), formaldehyde (1%), and tannic acid (1%) fixative with sucrose as an osmotic agent (35). This method of fixation was chosen to prevent possible disturbances of the air space distribution of deposited materials and maintaining physiological inflation levels comparable to that of the end-expiratory volume. This was performed using protocols previously employed to study pulmonary effects of SWCNT (47). Briefly, animals were deeply anesthetized with an overdose of sodium pentobarbital, the trachea was cannulated, and laparotomy was performed. Mice were then euthanized by exsanguination. The pulmonary artery was cannulated via the ventricle, and an outflow cannula was inserted into the left atrium. In quick succession, the tracheal cannula was connected to a 5 cmH_2O pressure source, and clearing solution (saline with 100 U/ml heparin, 350 mosM sucrose) was perfused to clear blood from the lungs. The perfusate was then switched to the fixative. Fixed lung volume was measured by water displacement (49). Coronal sections were cut from the lungs. The lungs were embedded in paraffin and sectioned at a thickness of 5 μm with an HM 320 rotary microtome (Carl Zeiss, Thornwood, NY). Lung sections for histopathological evaluation were stained with hematoxylin and eosin and examined by a board certified veterinary pathologist for morphological alterations.

Sirius red staining. The distributions of type I and III collagen in the lung tissue were determined by morphometric evaluation of the Sirius red-stained sections (47). Briefly, paraffin lung sections (5-μm thick) were deparaffinized and dehydrated. To identify collagen fibers under the microscope, the sections were stained with F3BA/picric acid for 1–2 h, washed with 0.01 N HCl for 1 min, and counterstained with Mayer's hematoxylin for 2 min. The slides were then dehydrated and mounted with coverslip (23). Type I and III collagen stained by Sirius red was visualized, and six randomly selected areas were scored under polarized microscopy using image analysis. With this morphometric method, the average thickness of Sirius red-positive connective tissues in the alveolar wall was quantitatively measured. Volume and surface density were measured using standard morphometric analyses of points and intercept counting (54). Average thickness of the Sirius red-positive connective tissues of the alveolar wall was computed from two times the ratio of volume density of points to the surface density of the alveolar wall.

Field emission SEM examination. For SEM, lung slices ~1-μm thick were taken from the fixative-preserved lungs, dehydrated in a graded series of alcohol, critical point-dried, and then carbon coated. After carbon coating, the specimens were examined with a field emission SEM (FESEM; model S-4800; Hitachi) operated at between 5 and 20 kV.

Lung collagen measurements. Total lung collagen content was determined by quantifying total soluble collagen using the Sircol Collagen Assay Kit (Accurate Chemical and Scientific, Westbury, NY). Briefly, whole lungs were homogenized in 0.7 ml of 0.5 M acetic acid containing pepsin (Accurate Chemical and Scientific) with 1:10 ratio of pepsin to tissue wet weight. Each sample was stirred vigorously for 24 h at 4°C and centrifuged, and 200 μl of supernatant was assayed according to the manufacturer's instructions.

Preparation of lung homogenates. The whole mouse lungs were separated from other tissues and weighed before being homogenized with a Tissue-Tearor (model 985-370; Biospec Products, Racine, WI) in PBS (pH 7.4) for 2 min. The homogenate suspension was frozen at −80°C until processed.

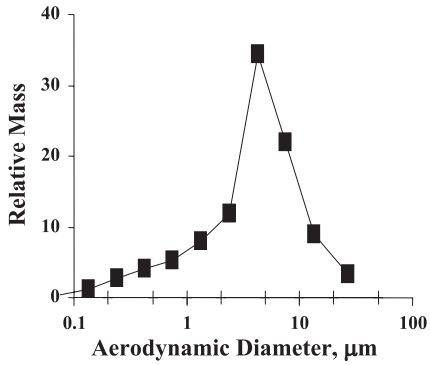

Fig. 1. Single-walled carbon nanotubes (SWCNT) size distribution measured with cascade impactor. The mass mode aerodynamic diameter is 4.2 μm.

HPLC assay of malondialdehyde. Accumulation of lipid peroxidation products was assessed by accumulation of malondialdehyde (MDA). MDA was analyzed by HPLC using a procedure described by Young and Trimble (56). Briefly, MDA was analyzed in lung homogenates following a reaction with thiobarbituric acid and phosphoric acid. A Waters HPLC system with a 717 Autosampler, a Waters Nova-Pak C18 column (5 μm, 150 × 3.9 mm), a Waters 600 controller pump, and a 474 fluorescence detector was used to measure MDA in samples. The wavelengths employed in the assay were 532 nm (excitation) and 553 nm (emission). Eluent was 25 mM phosphate buffer:CH_3OH (1:1 vol/vol) at pH 6.5, and the flow rate was 0.8 ml/min. Under these conditions, the retention time for MDA was 6.5 min. The data acquired was exported from the Waters 474 detector and analyzed using Millennium 2000 software (Waters, Milford, MA).

Fluorescence assay for low molecular weight thiols. Low molecular weight thiol concentration in lung homogenates was determined using ThioGlo-1, a maleimide reagent, which produces a highly fluorescent adduct on its reaction with SH- groups (46). Low molecular weight thiol content was estimated by an immediate fluorescence response registered on addition of ThioGlo-1 to the lung homogenate. A CytoFluor multiwell plate reader Series 4000 (Applied Biosystems, Foster City, CA) was employed for the assay of fluorescence using excitation at 360/40 nm and emission at 530/25 nm with a gain of 50. The data obtained were exported and analyzed using CytoFluor Software (Applied Biosystems).

Quantitative measurement of total antioxidant status in the lung homogenates. Lung total antioxidant status was determined using the NWLSS Antioxidant Reductive Capacity Assay (Northwest Life Science Specialties, Vancouver, WA). Briefly, the test is based on the ability of antioxidants in the lung homogenate to reduce Cu^{2+} to Cu^{+}, which reacts with bathocuproine to form a complex with maximal absorbance at 490 nm. Absorbance was measured before and after addition of bathocuproine. A standard curve was generated using uric acid.

Measurement of protein carbonyls in the lung homogenates. The quantity of oxidatively modified proteins assessed by measurement of protein carbonyls in lung homogenates was determined using the Biocell PC ELISA kit (Northwest Life Science Specialties). Sensitivity of assay is <0.1 nmol/mg protein.

Measurement of pulmonary function. Spontaneous breathing patterns were monitored using whole body plethysmography. Breathing patterns were monitored 24 h before SWCNT exposure (baseline) and then 1, 7, and 28 days following inhalation to detect treatment-related changes. Mice were acclimated to the plethysmograph for 10 min followed by 30 min of acquisition of spontaneous breathing data. Expiratory and inspiratory time, frequency, and relaxation time were calculated from the raw waveforms using BioSystem XA software version 2.0.248 (Buxco Electronics, Wilmington, NC) and expressed as percentage of control air-exposed mice.

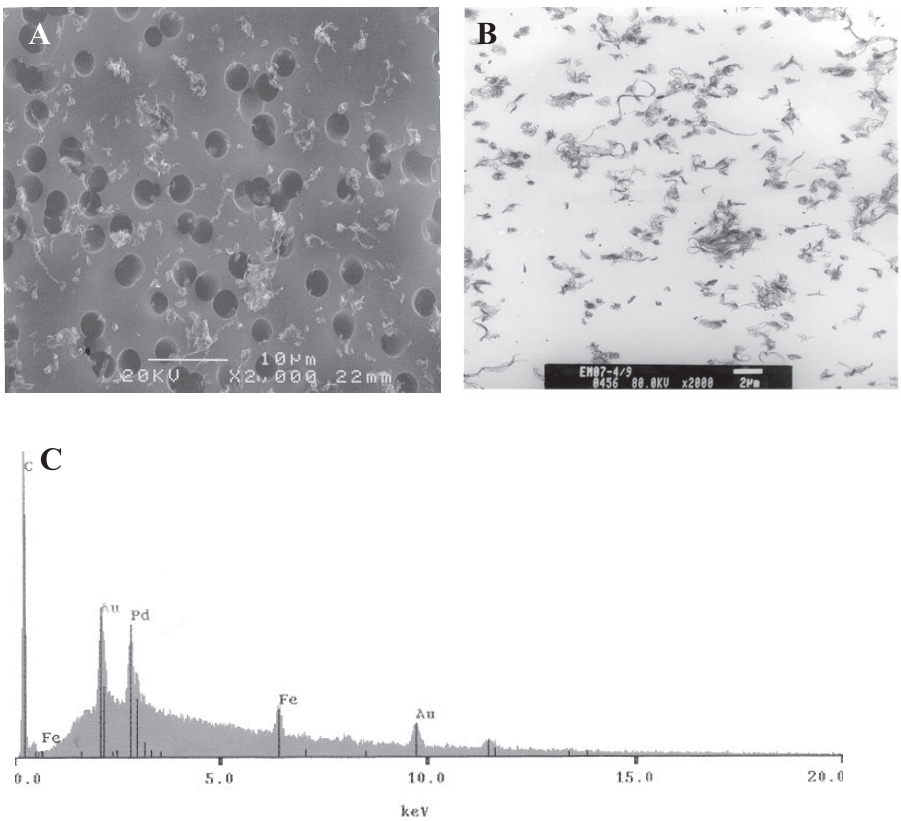

Fig. 2. *A*: representative scanning electron micrograph (SEM) of the SWCNT particles collected on stage 9 of the Micro-Orifice Uniform Deposit Impactor (MOUDI) impactor system (median aerodynamic diameter of 240 nm). *B*: representative transmission electron micrograph of SWCNT particles collected on stage 9 of a MOUDI (median aerodynamic diameter of 240 nm). *C*: SEM-EDS analysis of a SWCNT particle.

K-ras mutation analysis. For mutation analysis, three successive lung sections were prepared from each mouse lung tissue paraffin-embedded block, combined, and treated with xylene/ethanol to eliminate the paraffin. DNA was extracted from each sample using the protocol combining proteinase digestion and phenol/chloroform extraction. DNA was recovered by ethanol precipitation and resuspension in distilled water and kept at −20°C until analyzed. A sensitive K-*ras* mutation detection method was used to combine nested PCR, mutant allele enrichment by *Ban*I restriction enzyme digestion, and denaturing gradient gel electrophoresis (DGGE) to separate mutant alleles from wild-type alleles as previously described by Stabile et al. (50). Each mutant allele was isolated from the gel and further characterized by automated sequencing to determine the nature of the mutation.

Statistics. Treatment-related differences were evaluated using two-way ANOVA, followed by pairwise comparison using the Student-Newman-Keuls tests as appropriate. Statistical significance was considered at $P < 0.05$. Data are presented as means ± SE.

Statistical analysis for the mutation data was performed using a χ^2 test; the data were analyzed as counts (proportions) of mutations and no mutations among mice in a number of treatment/time groups. A P value ≤0.05, at least one of the proportions in that particular analysis, was considered statistically significant, although a valid χ^2 test requires expected counts in each cell of the analysis table to be ≥5.

RESULTS

Mass concentration and particle size distribution. SWCNT concentration within the exposure chambers was monitored in real-time by a DataRAM to allow feedback control. Gravimetric samples were taken every 15 min at two sites within each exposure chamber using 25-mm cassettes and PVC filters at a flow rate of 1 l/min. The mean SWCNT concentration determined by the gravimetric samples was 5.52 ± 1.37 mg/m^3 (mean ± SD). SWCNT mass mode aerodynamic diameter was ~4.2 μm determined by measuring the iron content of filters from various stages of a MOUDI cascade impactor (Fig. 1); the distribution was skewed to smaller particle sizes.

Pulmonary deposited dose. The pulmonary deposited dose per animal was derived by the formula

$$\text{Deposited dose} = (\text{aerosol concentration}) \times (\text{exposure duration}) \times (\text{minute ventilation}) \times (\text{deposition fraction})$$

where the target aerosol concentration was 5 mg/m^3, and the exposure duration was 20 h (5 h/day for 4 days) in this study. The mean minute ventilation was estimated to be 165 cm^3/min according to the information provided by The Jackson Laboratory database (http://phenome.jax.org/pub-cgi/phenome/mpdcgi?rtn=meas/catlister&req=Crespiratory). Note that there are wide variations in both the tidal volumes and breathing rates of mice depending on how these values were measured; therefore, the minute ventilation value used here is a best estimate. The deposition fraction of aerosol particles in the mouse pulmonary region depends on the particle size distribution of the aerosol and was determined to be 0.5% (42). The value was calculated based on the size characterization of SWCNT aerosols during the animal exposure (2). By substituting all the values into the formula, the deposited dose in the pulmonary region of the mouse respiratory tract was ~5 μg.

Particle morphology. SWCNT particles were collected on polycarbonate filters (for SEM) and microscope grids (for TEM) placed on different stages of MOUDI. Representative SEM and TEM images of SWCNT particles are shown in Fig. 2, *A* and *B*, respectively. Particles with different morphologies shown on the micrographs indicate that, even though their shapes and structures were different, they had similar aerodynamic behavior and thus were collected on the same MOUDI stage. Results from a series of SEM and TEM micrographs both indicate that there was a distinctive trend of decreasing particle size for particles collected on a lower stage of the MOUDI. This demonstrates that the strategy of using stages with and without oil-soaked filters alternately worked well for collecting SWCNT particles without the phenomena of particle bounce or reentrainment. By counting the images of the particles on the micrographs, the stage with the cutoff of 0.18 μm had the highest counts, indicating that the count mode aerodynamic diameter was ~240 nm. This demonstrates that the aerosol produced by our generator contained a high number of nano-sized SWCNT structures. The SEM-EDS analysis

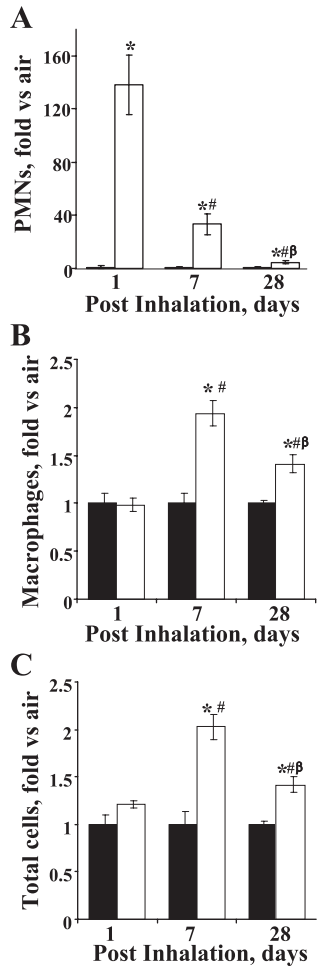

Fig. 3. Cell profile in bronchoalveolar lavage (BAL) fluids of C57BL/6 mice after inhalation of SWCNT (5 mg/m^3, 5 h/day, 4 days). *A*: polymorphonuclear leukocytes (PMNs). *B*: alveolar macrophages. *C*: total cells. Black columns: air exposure. White columns: inhalation exposure with SWCNT. Average absolute values from air-exposed control mice were (0.99 ± 0.35) × 10^3, (5.04 ± 0.32) × 10^5, and (5.05 ± 0.32) × 10^5 for PMNs, macrophages, and total cells, respectively, throughout recovery time. Means ± SE (n = 12 mice per group). *$P < 0.05$ vs. control air-exposed mice; #$P < 0.05$ vs. 1 day after last inhalation with SWCNT; β$P < 0.05$ vs. 7 days after last inhalation with SWCNT.

Table 1. *Inflammatory responses to SWCNT (24-h post-pharyngeal aspiration)*

	5 μg Per Mouse	10 μg Per Mouse	20 μg Per Mouse
PMNs, fold vs. control	36.8±2.5*	51.0±9.6*	72.4±5.4*†‡
LDH, % of control	196.4±12.7*	245.1±15.4*†	286.0±11.4*†‡
Protein, % of control	111.5±3.4*	135.0±3.5*†	191.9±4.6*†‡
TNF-α, fold vs. control	5.3±1.8*	6.8±1.5*	13.1±1.9*†‡
IL-6, % of control	146.5±53.8	351.6±47.9*†	851.0±97.9*†‡

Values are means ± SE. *$P < 0.05$ vs. control PBS-aspirated mice; †$P < 0.05$ vs. mice aspirated with 5 μg per mouse single-walled carbon nanotubes (SWCNT); ‡$P < 0.05$ vs. mice aspirated with 10 μg per mouse SWCNT. Average absolute values from control air-exposed mice were (0.48 ± 0.17) × 10^3 cells, 11.9 ± 0.4 U/l, 0.163 ± 0.006 mg/ml, 1.4 ± 0.6 pg/ml, and 2.7 ± 1.1 pg/ml for polymorphonuclear leukocytes (PMNs), lactate dehydrogenase (LDH), protein, TNF-α, and IL-6, respectively.

(Fig. 2*C*) indicates that the particles were composed of mostly carbon with a fair amount of iron (Au and Pd were the sputter coating materials).

Characterization of inflammatory response. To characterize the lung injury and inflammatory responses to SWCNT particles, we compared cell differential and total cell counts in the BAL fluids of C57BL/6 mice, permeability of the lung epithelium was assessed by protein levels, cell damage was evaluated by the release of LDH, and lung histopathology was performed on *days 1*, *7*, and *28* after inhalation or pharyngeal aspiration exposure to SWCNT.

BAL cytology indicated a robust but transient accumulation of neutrophils after inhalation exposure to SWCNT with maximum on *day 1* posttreatment with values returning toward control thereafter (Fig. 3*A*). An increased number of AM (Fig. 3*B*) and of total cells (Fig. 3*C*) reaching a maximum on *day 7* postexposure was documented. Although inflammation returned toward control 28 days postinhalation, at this time point, PMNs, AM, and total cell numbers in BAL fluid remained significantly (7.1-, 1.4-, and 1.4-fold) elevated compared with the air control group, respectively. Dose-dependent increased levels of PMNs were found following pharyngeal aspiration of 5–20 μg per mouse SWCNT (Table 1). Time course of inflammatory cell accumulation in BAL fluid of mice exposed by pharyngeal aspiration to SWCNT (10 μg per mouse) revealed the highest response in PMN numbers on *day 1* and AM on *day 7* (Table 2). Notably, pharyngeal aspiration of 20-μg SWCNT resulted in a lower level of PMNs accumulation in BAL fluid 1 day postexposure compared with inhalation exposure with lung burden of 5 μg per mouse (Table 1 and Fig. 3*A*).

Changes in lung permeability were assessed by the level of protein in the BAL fluid. Time course of protein accumulation in BAL fluid of mice after inhalation of SWCNT revealed a significant 68%, 47%, and 33% increase over control groups throughout recovery time of 1, 7, and 28 days postexposure (Fig. 4*A*). Increased lung permeability observed after SWCNT aspiration was dose-dependent (Table 1). Pharyngeal aspiration with SWCNT at a dose of 10 μg per mouse increased BAL protein to a lesser extent than inhalation (burden 5 μg) relative to their respective controls on *day 1* postexposure (Table 2 and Fig. 4*A*).

The degree of pulmonary cytotoxicity caused by SWCNT inhalation or pharyngeal aspiration was assessed by LDH activity in the BAL fluid recovered from mice. Time course of LDH accumulation in BAL fluid of mice that inhaled SWCNT revealed a significant 118%, 80%, and 71% increase over

Table 2. *Comparing aspiration and inhalation exposures*

	Aspiration, 10 μg per mouse	Inhalation, 5 mg/m³, 5 h/day, 4 days
	1 day postexposure	
PMNs, fold vs. control	51.0±9.6	147.4±18.9
LDH, % of control	245±15	218±26
Protein, % of control	135±3.5	168±3.0
TNF-α, pg/ml	9.5±2.1	10.8±4.7
IL-6, pg/ml	9.6±1.3	16.2±5.9
TGF-β, fold vs. control	1.52±0.09	3.1±0.11
Collagen, % of control	126±2.5	171±3.5
	7 day postexposure	
PMNs, fold vs. control	26.4±10.2	55.7±13.2
AM, % of control	212.2±14.7	194.0±13.3
TGF-β, fold vs. control	2.0±0.1	7.9±0.4
Collagen, % of control	153±12	227±7
	28 day postexposure	
Collagen, % of control	188±11	313±18

Values are means ± SE. TGF-β, transforming growth factor-β; AM, alveolar macrophages.

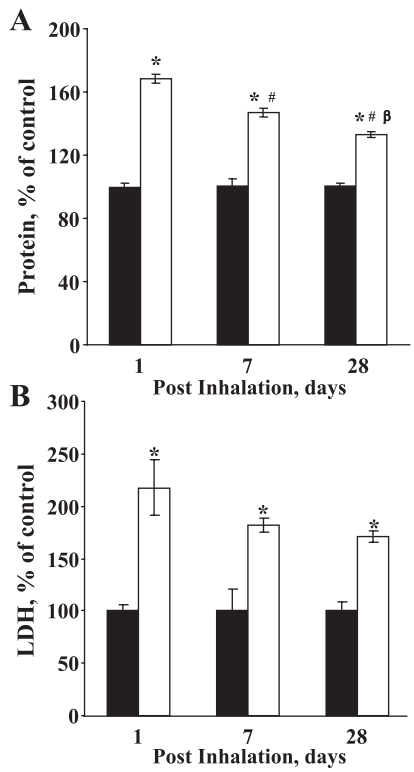

Fig. 4. Damage to pulmonary cells evaluated by changes in the level of protein (*A*) and lactate dehydrogenase (LDH) activity (*B*) in BAL fluid of C57BL/6 mice after inhalation of SWCNT (5 mg/m³, 5 h/day, 4 days). Black columns: air exposure. White columns: inhalation exposure to SWCNT. Average absolute value of protein content from air-exposed control mice was 0.29 ± 0.01 mg/ml throughout recovery time. LDH average absolute values from air-exposed control mice were 65.2 ± 3.8, 12.3 ± 2.8, and 19.2 ± 1.7 U/l throughout recovery time of 1, 7, and 28 days postexposure, respectively. Means ± SE ($n = 12$ mice per group). *$P < 0.05$ vs. control air-exposed mice; #$P < 0.05$ vs. 1 day after last inhalation with SWCNT; β$P < 0.05$ vs. 7 days after last inhalation with SWCNT.

control groups throughout recovery time (1, 7, and 28 days postexposure; Fig. 4*B*). Dose-dependent increased levels of LDH were found following pharyngeal aspiration of 5–20 μg per mouse SWCNT (Table 1). The pulmonary cytotoxicity response after SWCNT (10 μg per mouse) aspiration observed on *day 1* was not different from inhalation of 5 μg of SWCNT (Table 2 and Fig. 4*B*).

Histopathology. Morphological alterations in lungs from mice inhaling SWCNT were evaluated by a board-certified veterinary pathologist. The principal histopathological alterations in mice inhaling SWCNT were pulmonary inflammation, bronchiolar epithelial cell hypertrophy, and the presence of green-brown foreign material in the interstitium, intracellularly within individual macrophages or free of lung tissue and most frequently aggregated near bronchoalveolar junctions, often with associated AM (Fig. 5 and Table 3). Histopathological changes tended to be centered near the 1st generation alveolar ducts. Bronchiolar epithelial cell changes in the inhalation study were principally bronchiolar epithelial cell hypertrophy. Compared with the normal bronchiolar epithelium observed in control mice (Fig. 5*A*) 1-day postexposure group, hypertrophy was accompanied by hyperplasia. These foci of hypertrophy and hyperplasia were most frequently manifested as increased nuclear size, increased cytoplasmic volume, increased cytoplasmic basophilia, and occasional mitotic figures (Fig. 5, *A* and *D*). At 7 days postexposure, foci of bronchiolar epithelial cell hypertrophy were observed in all exposed mice, but hyperplasia was associated with hypertrophy in only one mouse. At 28 days postexposure, four of the five exposed mice had bronchiolar epithelial cell hypertrophy with one mouse having both hypertrophy and hyperplasia, one mouse having peribronchiolar bronchiolization accompanying bronchiolar epithelial cell hypertrophy, and two mice having bronchiolar epithelial cell hypertrophy without other bronchiolar alterations. At 1 day after inhalation, inflammation was classified as histiocytic or histiocytic and neutrophilic (Fig. 5*B*). Throughout the postexposure time course, macrophages were the principal inflammatory cells (Fig. 5). An atypical mitotic figure was observed in one mouse at 7 days postexposure, and material consistent with SWCNT nanoropes intertwined with the abnormal mitotic figure (Fig. 5*C*). This suggests the potential for SWCNT to interfere with the mitotic spindle. In addition, macrophages occasionally did not have nuclei. These anuclear macrophages often had increased cytoplasmic eosinophilia and were not observed in control mice or at 1 day post-SWCNT inhalation but were noted in four of five mice 7 days postexposure and in five of five mice at 28 days postexposure (Fig. 5*D* and Table 3). The anuclear macrophages suggested either abnormal mitoses or an apoptotic process involving karyolysis. By 28 days postexposure, foci of granulomatous inflammation were often well-organized (Fig. 5*E*) with fibrosis seen in sections stained with Masson's trichrome (Fig. 5*F*). Histopathological changes are summarized in Table 3. As demonstrated by histopathology and illustrated by FESEM examination of lung specimens (Fig. 6), inhalation exposure to SWCNT produced granulomatous inflammation in

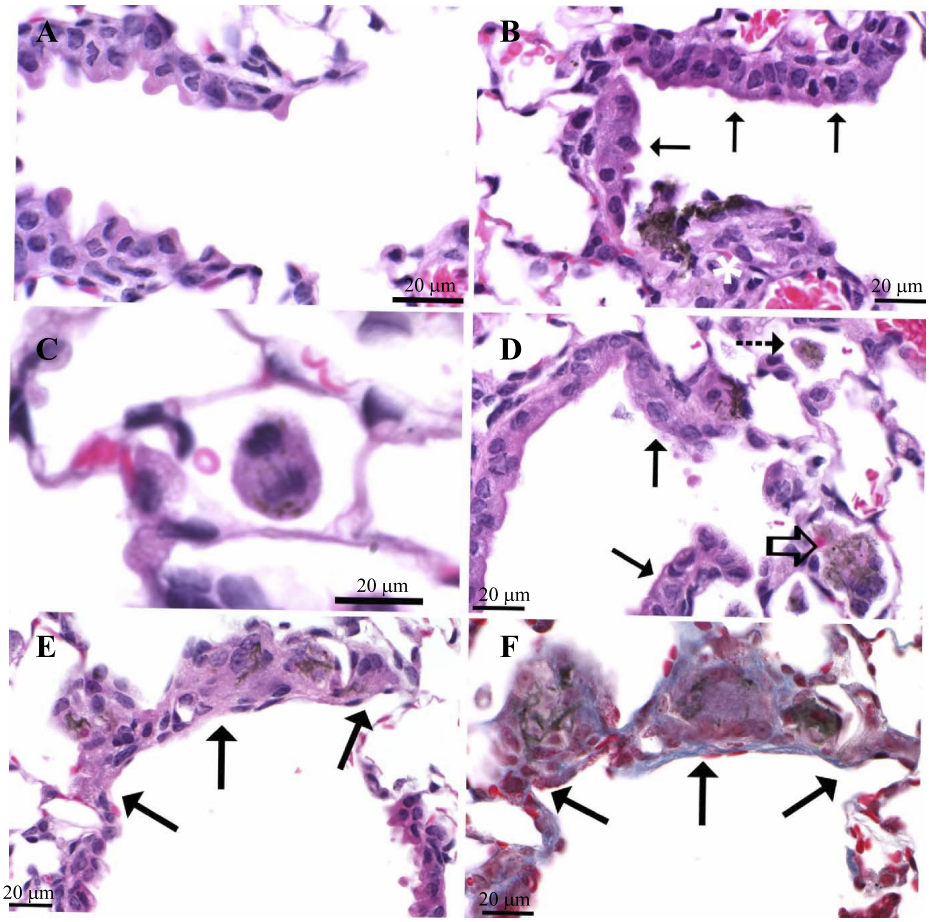

Fig. 5. Histopathology of lung sections from the SWCNT inhalation study (5 mg/m^3, 5 h/day, 4 days). *A*: normal bronchioloalveolar junction in a control mouse. *B*: bronchiolar epithelial cell hypertrophy (solid arrows) and histiocytic inflammation (*) 1 day after the last SWCNT exposure. *C*: 7 days after the last SWCNT exposure, an anaphase bridge in a dividing macrophage containing SWCNT suggests the potential for interference with the mitotic spindle. *D*: organized epithelioid macrophages (open arrow), an eosinophilic macrophage containing SWCNT that does not have a nucleus and has an indistinct cytoplasmic membrane consistent with cell death (dashed arrow), and bronchiolar epithelial hypertrophy (solid arrows) 28 days after the last SWCNT exposure. *E*: granulomatous inflammation (solid arrows) at the bronchioloalveolar junction 28 days after SWCNT inhalation. *F*: early fibrosis is indicated by blue staining in this Masson's trichrome-stained section of the lung shown in *E*.

Table 3. *Prevalence and mean severity of histopathological alterations in lungs of mice inhaling SWCNT*

Postexposure Duration/Histopathological Changes	1 Day		7 Days		28 Days	
	Control*	SWCNT*	Control*	SWCNT*	Control*	SWCNT*
Inflammation	0/5 (0±0)	5/5 (5.1±0.1)	0/5 (0±0)	5/5 (5.0±0)	0/5 (0±0)	5/5 (5.0±0)
Anuclear macrophages	0/5 (0±0)	0/5 (0±0)	0/5 (0±0)	4/5 (0.8±0.2)	0/5 (0±0)	5/5 (1.0±0)
Bronchiolar epithelial changes†	0/5 (0±0)	5/5 (4.3±0.7)	0/5 (0±0)	5/5 (4.5±0.3)	0/5 (0±0)	4/5 (3.1±0.9)

*Prevalence (mean severity ± SE); †includes changes classified as hypertrophy with and without hyperplasia or peribronchiolar bronchiolization.

the alveolar region of the lungs. Following the exposure, the epithelioid macrophages develop an extensive system of fingerlike projections over the surface of the granulomas 28 days postexposure (Fig. 6).

Cytokines. The most significant induction of proinflammatory cytokines was observed in BAL fluids of C57BL/6 mice 1 day postinhalation of SWCNT (Fig. 7, *A* and *B*). At this time point, levels of TNF-α and IL-6 were 4.4- and 7.9-fold higher compared with air control groups, respectively. Dose-dependent increased levels of TNF-α and IL-6 were found following pharyngeal aspiration of 5–20 μg per mouse SWCNT (Table 1). No significant difference in the levels of proinflammatory cytokines was found between aspiration of 10 μg of SWCNT and inhalation with lung burden of 5 μg. Significant elevation of TGF-β1 release was found in BAL fluid of C57BL/6 mice after SWCNT inhalation throughout the recovery time course (Fig. 7*C*). Maximal fibrogenic TGF-β1 release after SWCNT inhalation was observed on *day 7* and was significantly greater than after aspiration of 10-μg SWCNT (Table 2).

Collagen deposition and morphometric changes. Collagen deposition and pulmonary fibrosis are typical features of inflammatory response to various injuries to the lung, including particles. The time course of collagen accumulation in lung of C57BL/6 mice after inhalation of SWCNT revealed a significant 71%, 127%, and 182% increase over air control groups at 1, 7, and 28 days postexposure, respectively (Fig. 8*A*). Evaluation of fibrosis after pharyngeal aspiration with 10 μg per mouse of SWCNT showed significantly less collagen deposition compared with SWCNT inhalation with a lung burden of 5 μg per mouse (Table 2).

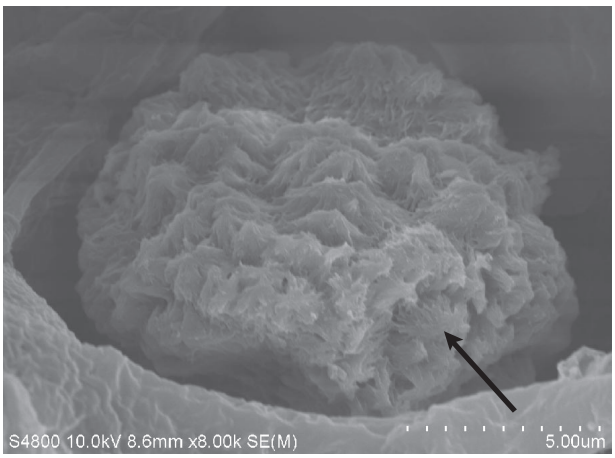

Fig. 6. Field emission SEM (FESEM) image of granulomatous inflammation in the alveolar region at 28 days after inhaling SWCNT (5 mg/m^3, 5 h/day, 4 days). Arrow indicates fingerlike projections that are typical of the epithelioid macrophages that form the granulomas.

Morphometric changes in alveolar wall collagen fiber content after inhalation exposure are presented in Fig. 8*B*. Results from determination of the average thickness of alveolar connective tissue at various recovery times after inhalation of SWCNT revealed increased thickness at *day 1* postinhalation,

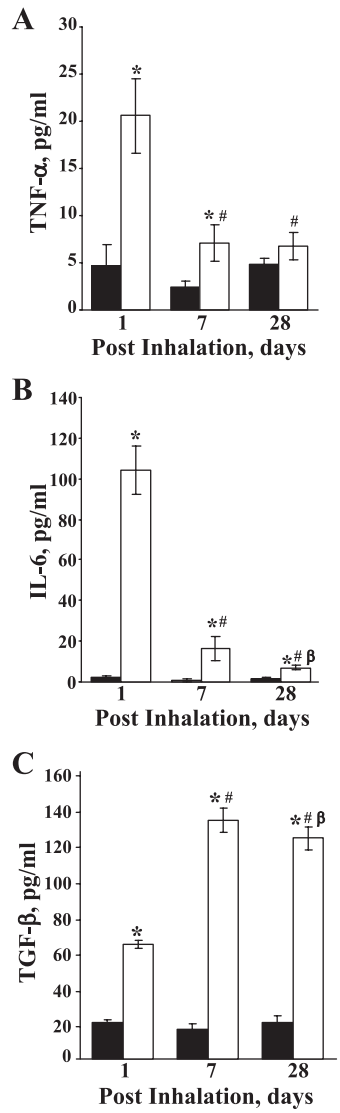

Fig. 7. Accumulation of proinflammatory and fibrogenic cytokines in BAL fluids of C57BL/6 mice after inhalation of SWCNT (5 mg/m^3, 5 h/day, 4 days). *A*: TNF-α. *B*: IL-6. *C*: transforming growth factor-β1 (TGF-β). Black columns: air exposure. White columns: inhalation exposure to SWCNT. Means ± SE (n = 12 mice per group). *$P < 0.05$ vs. control air-exposed mice; #$P <$ 0.05 vs. 1 day after last inhalation with SWCNT; β$P < 0.05$ vs. 7 days after last inhalation with SWCNT.

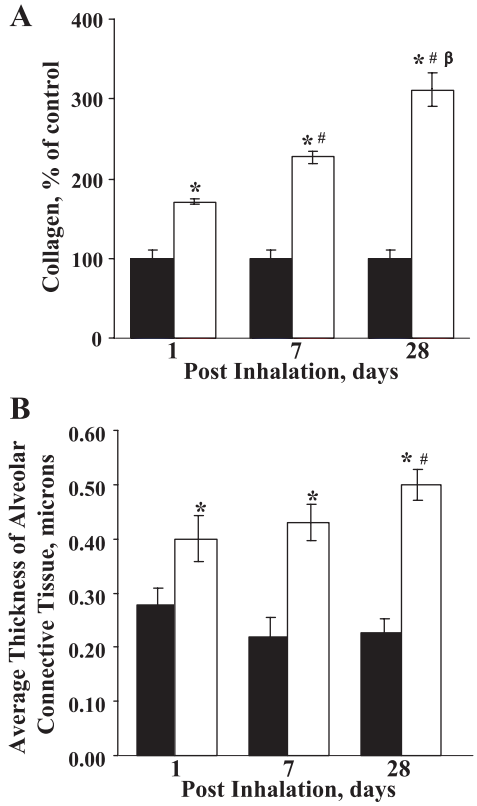

Fig. 8. Collagen accumulation (*A*) and morphometric changes in alveolar wall collagen fiber content determined as average thickness of alveolar connective tissue (*B*) in the lung of C57BL/6 mice after inhalation of SWCNT (5 mg/m^3, 5 h/day, 4 days). Black columns: air exposure. White columns: inhalation exposure to SWCNT. Collagen average absolute value from air-exposed control mice was 7.5 ± 0.6 μg/mg lung throughout recovery time. Means ± SE (n = 12 mice per group). *$P < 0.05$ vs. control air-exposed mice; #$P < 0.05$ vs. 1 day after last inhalation with SWCNT; β$P < 0.05$ vs. 7 days after last inhalation with SWCNT.

which progressed further by *day 28* compared with air control groups. Light micrograph of Sirius red-stained lung section from SWCNT inhalation exposed lung demonstrating the broad distribution of SWCNT from alveoli at the bronchiole junction to the more distal regions of the lungs (Fig. 9*A*). Light micrograph of a proximal alveolar region following inhalation exposure to SWCNT demonstrates a high concentration of SWCNT that is in the early stages of granuloma development on *day 1* postexposure (Fig. 9*B*).

Pulmonary functions. Exposure to a lung irritant can lead to changes in breathing pattern. SWCNT inhalation caused minor changes in breathing pattern. Elevated breathing frequency was detected in C57BL/6 mice after inhalation with SWCNT throughout recovery time compared with air control mice (Fig. 10). This change was accompanied by decreases in the inspiratory, expiratory, and relaxation time as early as *day 1* following SWCNT inhalation and persisted for at least 28 days compared with air-exposed animals (Fig. 10).

Oxidative stress in the lung. The level of oxidative damage in the lung caused by SWCNT inhalation was assessed by GSH, protein thiols, lipid peroxidation products, total antioxidant capacity, and oxidatively modified proteins measured as protein carbonyls (Fig. 11). Time course of GSH depletion in the lung of mice that inhaled SWCNT revealed no changes 24 h after the last exposure and a significant 10% decrease from control at 7 and 28 days postexposure (Fig. 11*A*). Changes in the level of protein thiols in the lung of mice after inhalation of SWCNT revealed a significant 15%, 10%, and 9% decrease from control at 1, 7, and 28 days postexposure, respectively (Fig. 11*A*). Level of lipid peroxidation products measured as MDA showed a significant 21%, 31%, and 44% accumulation over control groups throughout the time course of 1, 7, and 28 days postexposure, respectively (Fig. 11*A*). Inhalation exposure to SWCNT resulted in a significant 22% and 10% depletion of total antioxidant capacity at 1 and 7 days posttreatment, which returned to the control level by 28 days postexposure (Fig. 11*B*). Significant elevation of the levels of protein carbonyls (5.6-, 4.0-, and 4.0-fold increases) was consistently observed after inhalation exposure of SWCNT at 1, 7, and 28 days posttreatment, respectively (Fig. 11*C*).

K-ras mutations in C57BL/6 mice. To assess genotoxicity of SWCNT, accumulation of K-*ras* mutations after the inhalation and aspiration exposure was evaluated. An example of K-*ras* mutation analysis by DGGE is shown in Fig. 12. The DGGE reveals the patterns of three different K-*ras* mutant alleles

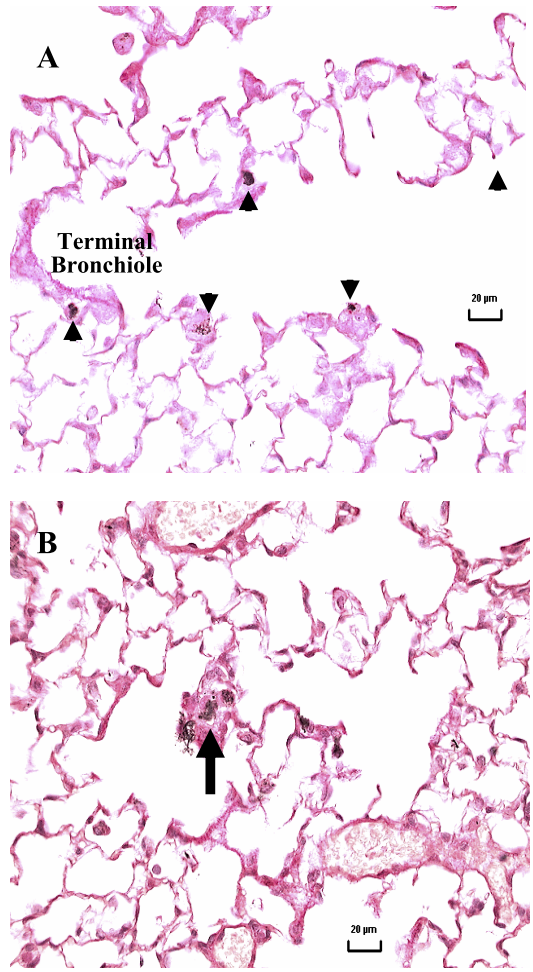

Fig. 9. Light micrographs of Sirius red-stained lung section from mice 1 day after inhalation of SWCNT (5 mg/m^3, 5 h/day, 4 days) demonstrating the broad distribution of SWCNT from alveoli at the bronchiole junction to the more distal regions of the lungs (*A*) and a high concentration of SWCNT that is in the early stages of granulomas development in a proximal alveolar region (*B*). Arrows indicate inhalation deposition sites of the SWCNT.

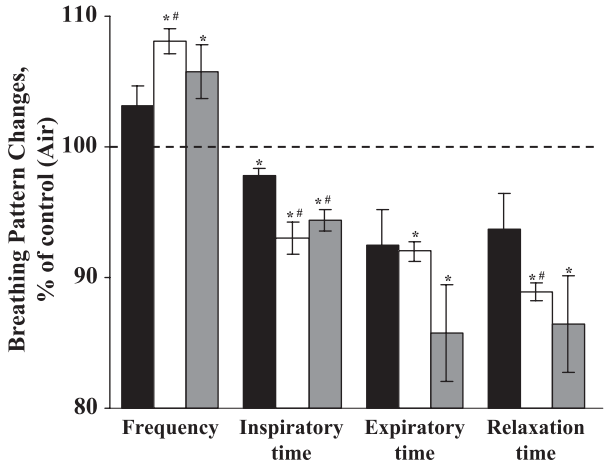

Fig. 10. Changes in breathing pattern after inhalation exposure of SWCNT (5 mg/m^3, 5 h/day, 4 days). Black columns: 1 day after last inhalation exposure. White columns: 7 days after last inhalation exposure. Gray columns: 28 days after last inhalation exposure Means ± SE (n = 12 mice per group). *$P < 0.05$ vs. control air-exposed mice; #$P < 0.05$ vs. 1 day after last inhalation with SWCNT.

detected in this study, the first two consisting of a change of the wild-type codon 12 (GGT, glycine) to an AGT (serine, *lane 2*) and a GAT (aspartate, *lane 3*). The third mutant allele (*lane 4*) contains a double mutation, including a GGT to GAT (aspartate) at codon 12 and a GTG to ATG at codon 8 (valine to methionine). K-*ras* mutations identified in tissue sections prepared from lungs of C57BL/6 mice in this study are summarized in Table 4. These mutations were found in mice treated with SWCNT by inhalation, whereas aspiration caused a low frequency of mutations that did not differ from untreated controls. Taken together, the results of these studies indicate a trend that a difference in the proportion of mutations exists among some of the various treatment/time groups. Particularly, the mutation proportion is higher among the mice treated with SWCNT by inhalation route and euthanized at both 7 and 28 days postexposure, compared with that in mice treated with SWCNT by aspiration. Interestingly, one of the mutations consists of a double mutation in codons 12 and 8 of the K-*ras* gene in mice at *day 28* postinhalation. These mutations have not been reported previously and may be specific for the SWCNT-exposure.

DISCUSSION

Deep penetration of nanotechnologies and nanomaterials into essentially all spheres of our life and a large number of nanoparticle-containing consumer products raise concerns about their undetermined and possibly damaging health effects (12, 13, 21, 28, 55). This concern is enhanced by unique physicochemical properties of nanomaterials potentially associated with unique effects on living matter and life (29). Of the many different types of nanomaterials, carbon nanotubes, particularly SWCNT, have the potential for diverse and versatile applications (44). Accordingly, the toxicity of SWCNT to cells and whole animals has received more study than the toxicity of many other types of nanoparticles (5, 6, 16, 17, 19, 29, 34).

Our previous studies established that aspiration of highly purified SWCNT (without significant admixtures of transition metals such as iron) indeed caused unusual inflammatory responses in the lung of exposed animals: a truncated but strong acute phase response followed by an early onset and progressive fibrotic response (47). This was accompanied by disturbed breathing pattern (47) and increased susceptibility to pulmonary infection (48). Some argue that pharyngeal aspiration, a single exposure to a bolus of SWCNT, is an artificial exposure and that the bolus exposure may contribute to the

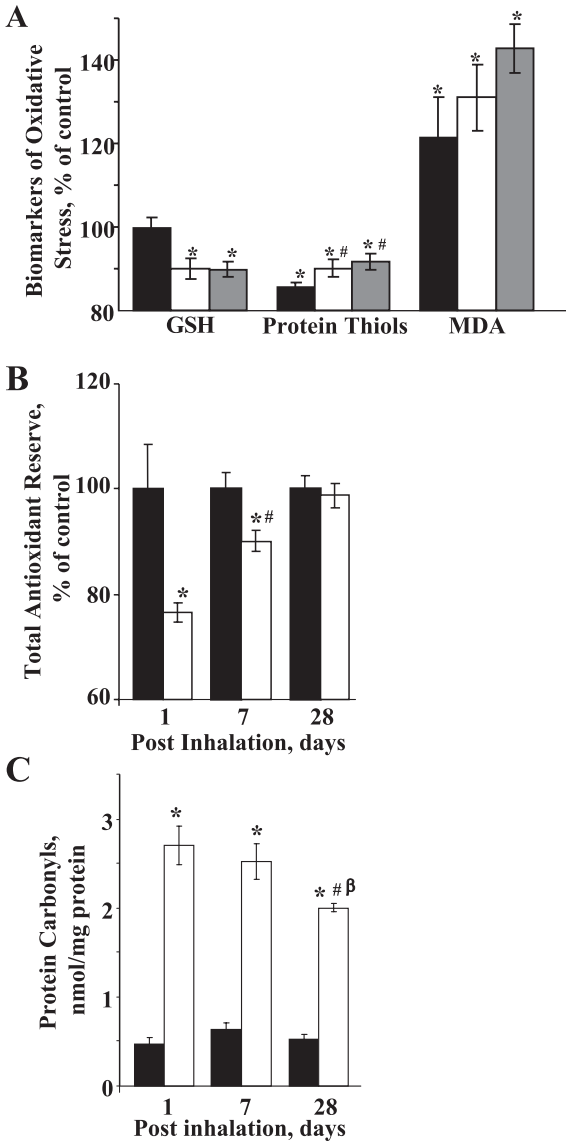

Fig. 11. Oxidative stress in the lung of mice after inhalation exposure of SWCNT (5 mg/m^3, 5 h/day, 4 days). *A*: biomarkers of oxidative stress in lung of mice after inhalation of SWCNT (black columns, 1 day after last inhalation exposure; white columns, 7 days after last inhalation exposure; gray columns, 28 days after last inhalation exposure). Average absolute values from air-exposed control mice for GSH, protein thiols, and malondialdehyde (MDA) were 14.0 ± 0.4 nmol/mg, 26.3 ± 0.5 nmol/mg, and 48.7 ± 0.8 pmol/mg, respectively, throughout recovery time. *B*: total antioxidant reserve in the lung of mice in response to inhalation of SWCNT (black columns, control air-exposed mice; white columns, SWCNT-exposed mice). Average absolute value for total antioxidant reserve from air-exposed control mice was 64.3 ± 3.2 nmol/mg throughout recovery time. *C*: level of carbonyls in the lung of mice after SWCNT inhalation (black columns, control air-exposed mice; white columns, SWCNT-exposed mice). Means ± SE (n = 12 mice per group). *$P < 0.05$ vs. control air-exposed mice; #$P < 0.05$ vs. 1 day after inhalation with SWCNT; β$P < 0.05$ vs. 7 days after inhalation with SWCNT.

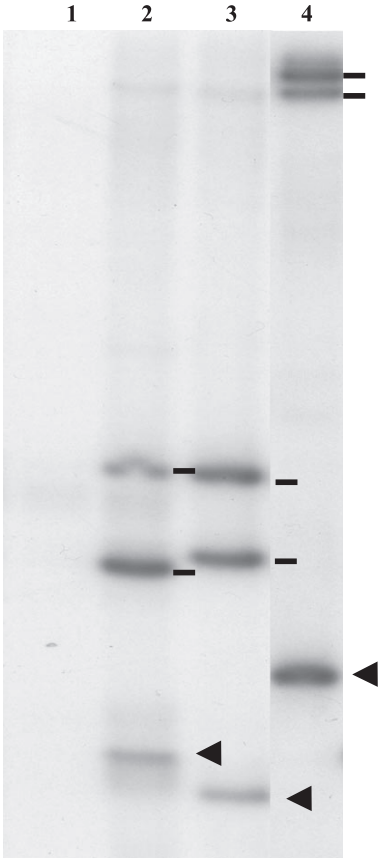

Fig. 12. An example of K-*ras* mutation analysis by denaturing gradient gel electrophoresis (DGGE). The gel shows 4 lanes (*lanes 1–4*) corresponding each to a specific pattern of K-*ras* mutant alleles from 4 different mouse lungs as separated by DGGE. Lung DNA sample 1 (*lane 1*) shows no mutation. Lung DNA samples 2, 3, and 4 each show a different mutation as revealed by the difference in their mutant band pattern, consisting of 1 mutant homoduplex (indicated by an arrowhead) at the *bottom* of the gel and the 2 respective mutant/wild-type heteroduplexes (each indicated by a line) in the *middle* (*lanes 2* and *3*) and at the *top* of the gel (*lane 4*). The 1st 2 mutations corresponded to a change at the wild-type K-*ras* gene codon 12 (GGT, glycine) to AGT (*lane 2*, serine) and GAT (*lane 3*, aspartate). The 3rd mutation is a double mutation consisting of a GGT to GAT (glycine to aspartate at codon 12) and a GTG to ATG (valine to methionine at codon 8). The type of mutation in each lane was determined by sequencing analysis of the mutant homoduplex band isolated from the gel.

pulmonary response. Moreover, aspiration studies reported thus far have been relatively high-dose exposures, which may not be relevant to chronic lower dose exposures in occupational settings (26). Before the current study, there was "no definitive inhalation study available that would avoid the potential for artifactual effects due to large aggregates forming during instillation exposure procedures" (10). Inhalation of SWCNT more closely mimics occupational and environmental settings than aspiration in that exposures are to more dispersed SWCNT structures and bolus effects are avoided. Therefore, we were eager to explore the pulmonary effects of inhaled SWCNT.

Technically, aerosolization of SWCNT and the inhalation exposures are very difficult because of their hydrophobicity and tendency to agglomerate yielding large entangled structures, often "bird's nest"-like, micrometer-size structures (33). As a result of formation of large agglomerates in suspension, asphyxia has been reported in rats following intratracheal instillation of poorly dispersed SWCNT (55). To avoid these substantial complications, we have developed special protocols and devices for adequate aerosolization of SWCNT (2). This technique included removing clumps, suspending by acoustic fluidization, breaking apart large agglomerates, and passing through a static discharger, settling chamber, and a cyclone (4-μm cutoff) to deliver SWCNT at a flow rate of 10 l/min. Application of our aerosolization technology resulted in the ability to obtain stable SWCNT aerosols with a concentration of 5 mg/m^3 with a count mode aerodynamic diameter of 240 nm.

Using the stable SWCNT aerosols, we were able to conduct inhalation studies to assess their pulmonary effects. The manufacturing of nanotube material relies on the use of transition metal catalysts. Redox active iron within carbonaceous particles may act as a catalyst of oxidative stress in biological settings. The major toxicity mechanisms induced by SWCNT include induction of inflammatory response and oxidative stress exacerbated by iron. Because inflammation provides a redox environment in which transition metals can fully realize their prooxidant potential, a combination of inflammatory response with catalytically competent metal-containing carbon nanotubes would synergistically enhance damage to cells and tissue. Therefore, in the current study, we chose to use nonpurified SWCNT containing up to 17.7% (weight) of iron for both inhalation and aspiration exposures. Assessment of nonpurified SWCNT employed in this study with purified SWCNT (0.2% of iron by weight) used in our previous study (47) shows that the higher content of iron was associated with enhancement of oxidative stress and some of the pulmonary responses. These include more pronounced decrease of content of low molecular weight thiols, elevated cell damage assessed by the release of LDH, and higher level of collagen deposition in the lung of animals exposed to SWCNT by aspiration.

Comparison of the inhalation protocols with previously reported results on aspiration showed that all unusual features of pulmonary response were retained or enhanced. That is, the short and strong acute inflammatory phase reaction was followed by a robust deposition of collagen leading to progressive fibrosis. Comparison of dose dependencies for aspiration exposures (5, 10, and 20 μg of SWCNT per mouse) with that for inhalation (deposited dose of 5 μg per mouse) showed that deposition of smaller SWCNT structures after inhalation resulted in cellular inflammation, LDH and protein release, and cytokine production two- to fourfold greater than those after aspiration exposure of larger SWCNT structures. Morphometric evaluation of Sirius red-stained lung sections revealed that SWCNT inhalation caused a fourfold increase in fibrosis compared with that seen after pharyngeal aspiration of SWCNT with collagen deposition in the peribronchial as well as interstitial areas. Overall, our results demonstrate that SWCNT inhalation exposure was much more potent than aspiration of a bolus dose of SWCNT. Interestingly, Mercer et al. (36) demonstrated a fourfold greater fibrotic potency after pharyngeal aspiration of a well-dispersed SWCNT compared with a less dispersed suspension. They associated this potency difference with a greater potential for smaller SWCNT structures to enter the alveolar walls and cause interstitial fibrosis. Thickening of alveolar walls has also been demonstrated in mice inhaling multiwalled carbon nanotubes (30).

Table 4. *K-ras mutations among the various groups of mice*

Type of Exposure	Recovery, days	Exposure	Mutation Incidence	Mutation Type, wild-type K-*ras* codon 12: GGT	Total
Inhalation	1	Air	0/5 (0.0%)		Air: 4/15 (26.7%)
		SWCNT	2/6 (33.3%)	1 GAT, 1 AGT	
	7	Air	2/5 (40.0%)	1 GAT, 1 AGT	
		SWCNT	4/5 (80.0%)	2 GAT, 2 AGT	SWCNT: 10/16 (62.5%)
	28	Air	2/5 (40.0%)	1 GAT, 1 AGT	
		SWCNT	4/5 (80.0%)	2 GAT, 1 AGT, 1 double mutation*	
Aspiration	7	PBS	0/3 (0.0%)		PBS: 1/8 (12.5%)
		SWCNT	0/3 (0.0%)		
	28	PBS	1/5 (20.0%)	1 GAT	SWCNT: 1/8 (12.5%)
		SWCNT	1/5 (20.0%)	1 AGT	

*The double mutation contains a GGT > GAT at codon 12 and a GTG > ATG at codon 8 of the K-*ras* gene. The χ^2 analysis of the proportion of mutations in the 6 treatment/time groups: 7 days/SWCNT/Aspiration (Asp), 7 days/SWCNT/Inhalation (Inh), 7 days/Sham, 28 days/SWCNT/Asp, 28 days/SWCNT/Inh, 28 days/Sham, $P = 0.045$, implying statistical significance. Note that there are 11 cells with expected counts <5. The χ^2 analysis of the proportion of mutations in the 3 treatment/time groups (7 days postexposure) with $P = 0.045$, implying statistical significance. Note that there are 5 cells with expected counts <5. The χ^2 analysis of the proportion of mutations in the 3 treatment/time groups (28 days postexposure) with $P = 0.075$. Note that there are 5 cells with expected counts <5. The χ^2 analysis of the proportion of mutations in the 3 treatment/time groups: 7 days/SWCNT/Inh, 28 days/SWCNT/Inh, 28 days/Sham, $P = 0.08$. Note that there are 5 cells with expected counts <5.

Inflammation and resulting fibrosis have been considered as significant risk factors in pulmonary carcinogenesis (20). Among the mutated genes implicated in pulmonary tumorigenesis, K-*ras* oncogene is frequently found in lung tumors of mice exposed to chemicals (8, 45). It was therefore important to investigate whether this gene mutation occurred after SWCNT exposure. We detected the increased rate of SWCNT-induced mutations that took place very early after SWCNT inhalation (on *days 1–7*) and persisted through *day 28*. The effect was coincident with the time of maximal inflammatory response suggesting that inflammation and resultant oxidative injury may be a cause of mutagenicity. Given that oxidative burst and accompanying oxidative stress are known to be significant contributors to genotoxicity, it is tempting to speculate that there is a causative association between accumulation of K-*ras* mutations and oxidative stress triggered by SWCNT inhalation. The types of mutations consisted of G-to-A transition that changes the wild-type codon 12 of the K-*ras* gene from GGT (glycine) to either AGT (serine) or GAT (aspartate). This type of mutation has been reported previously in lung tumors from susceptible mice (8, 45). For instance, lung tumors in mice exposed to the lung carcinogen, NNK [4-(methylnitrosamino)-1-(3-pyridyl)-1-butanone], showed a high proportion of this mutation that has been suggested to occur via the mutagenic lesions, including O^6-methylguanine, induced by NNK metabolites (8). Interestingly, one of the mutations found in SWCNT-treated mice (at *day 28* post-SWCNT inhalation) consisted of a double mutation occurring at codons 12 and 8 [GGT to GAT and GTG to ATG (valine to methionine), respectively]. The role of this double mutation is unknown and may be specific for SWCNT exposure.

Overall, these results are intriguing because K-*ras* mutations have been reported only in lung tumors from susceptible mice, such as the FVB/N mice, exposed to lung carcinogens (8, 45, 50). The K-*ras* gene is a member of the *ras* gene family consisting of the closely related H-, K-, and N-*ras* genes, which code for similar 21-kDa proteins (*ras*) that are involved in the signal transduction pathways. Activation of *ras* genes occurs with specific point mutations primarily at codon 12 and to a lesser extent at codons 13 and 61 and has been implicated in lung tumorigenesis (1, 22, 25). The significance of these low-fraction K-*ras* mutations in C57BL/6 mice is unknown. Several studies have shown an association between lung fibrosis and an increased risk of lung cancer (18, 20, 27). It was proposed that fibrosis might be involved in the carcinogenesis by the occurrence of atypical or dysplastic epithelial changes, which progressed to invasive malignancy (18). However, the involvement of K-*ras* mutations in fibrosis-associated lung cancer is not understood and merits further investigation. The detected mutations frequency of 62.5% (10/16) in mice after SWCNT inhalation is significantly higher than that in the untreated group of mice 26.7% (4/5). Further studies involving a bigger sample size may help in determining the usefulness of this gene mutation as a biomarker of exposure to SWCNT. Furthermore, the potential role in lung carcinogenesis requires further investigation by comparing C57BL/6 mice with other mouse strains susceptible to lung tumor formation.

Our results, which show that SWCNT inhalation induced unusual and robust inflammatory response and fibrosis, raise the question of the relevance of doses and conditions used in the current study to realistic human occupational exposures. Exposure to carbonaceous materials has been reported to cause pneumoconiosis in workers exposed to both natural and man-made graphite (37). Severe symptomatic cases with massive pulmonary fibrosis in the past were observed during carbon electrode production (45a). Mixed dust pneumoconiosis caused by long-term occupational exposure to graphite dust is a rare disease (9). Screening and clinical examination of 746 graphite workers revealed an elevated occurrence of upper respiratory tract infections, chronic bronchitis, and pneumonia (24). Hypertrophic laryngitis, papillomatous bronchitis, and angiofibroma of the larynx, considered to be precancerous lesions, have also been reported. However, recent reports emphasized that such exposures are likely to be associated with mixed dusts (45a).

Previously, we investigated the potential exposure levels of workers to SWCNT in a small-scale production setting (33). Under these conditions, the amount of material produced was very small (several grams), significant care was taken to reduce product loss during handling, and the observed airborne particle concentrations were low (with peak exposure of 53 $\mu g/m^3$). Agitation of the material by vortexing generated higher levels

of respirable SWCNT material. Thus, under large-scale manufacturing conditions, the potential for occurrence of occupational exposure may exist. In the current study, we observed that toxic outcomes of exposure of C57BL/6 mice to aerosolized respirable SWCNT (5 mg/m^3, 5 h, 4 days) resulted in a calculated lung burden of 5 μg per mouse. This lung burden would be achieved by workers exposed for <1 yr at the peak airborne concentrations measured in an occupational setting based on the studies of Maynard et al. (33). Our results may be important for establishing a permissible exposure level (PEL) for SWCNT. The exposure concentration, which we used in our inhalation studies, is the same as the current PEL set by Occupational Safety and Health Administration for respirable synthetic graphite dust, i.e., the PEL currently applied for SWCNT. Based on the outcomes of our inhalation study, it could be inferred that if workers were subjected to long-term exposures to respirable SWCNT at current PEL for synthetic graphite, they would likely have increased risk for pulmonary changes. Our results may be also compared with regulatory permissible levels established for ambient microparticles such as Environmental Protection Agency standard for $PM_{2.5}$, which is 65 μg/m^3 24 h daily and 15 μg/m^3 annual average (53).

Overall, our data suggest that outcomes of inhalation exposure to respirable SWCNT were very similar to those seen after pharyngeal exposure route leading to pulmonary toxicity. The chain of pathological events was realized through synergized interactions of inflammatory response and oxidative stress culminating in the development of multifocal granulomatous pneumonia, interstitial fibrosis, and mutagenesis. Because of exposure to smaller SWCNT structures by inhalation of a dry aerosol vs. aspiration of a particle suspension containing micrometer-size agglomerates, inhalation exposure was, in fact, more potent than aspiration of an equivalent mass of SWCNT.

ACKNOWLEDGMENTS

Expert technical assistance from D. Schwegler-Berry, S. Friend, D. Newcomer, J. Scabilloni, and L. Battelli is gratefully acknowledged. A. Mosley, M. Donlin, and J. Cumpston are acknowledged for their support as the inhalation exposure personnel.

GRANTS

This study was supported by NIOSH Grant OH008282, National Heart, Lung, and Blood Institute Grant HL-70755, National Occupational Research Agenda Grant 927000Y, and the 7th Framework Program of the European Commission.

DISCLAIMER

The findings and conclusions in this report are those of the authors and do not necessarily represent the views of the National Institute for Occupational Safety and Health.

REFERENCES

1. **Barbacid M.** *ras* genes. *Annu Rev Biochem* 56: 779–827, 1987.
2. **Baron PA, Deye GJ, Chen BT, Schwegler-Berry D, Shvedova AA, Castranova V.** Aerosolization of single-walled carbon nanotubes for an inhalation study. *Inhal Toxicol* 8: 751–760, 2008.
3. **Baughman RH, Galvao DS.** Crystalline networks with unusual predicted mechanical and thermal properties. *Nature* 365: 735–737, 1993.
4. **Baughman RH, Zakhidov AA, de Heer WA.** Carbon nanotubes–the route toward applications. *Science* 297: 787–792, 2002.
5. **Bergamaschi E, Bussolati O, Magrini A, Bottini M, Migliore L, Bellucci S, Iavicoli I, Bergamaschi A.** Nanomaterials and lung toxicity: interactions with airways cells and relevance for occupational health risk assessment. *Int J Immunopathol Pharmacol* 19: 3–10, 2006.
6. **Bianco A, Kostarelos K, Prato M.** Opportunities and challenges of carbon-based nanomaterials for cancer therapy. *Expert Opin Drug Deliv* 5: 331–342, 2008.
7. **Davoren M, Herzog E, Casey A, Cottineau B, Chambers G, Byrne HJ, Lyng FM.** In vitro toxicity evaluation of single walled carbon nanotubes on human A549 lung cells. *Toxicol In Vitro* 21: 438–448, 2007.
8. **Devereux TR, Belinsky SA, Maronpot RR, White CM, Hegi ME, Patel AC, Foley JF, Greenwell A, Anderson MW.** Comparison of pulmonary O^6-methylguanine DNA adduct levels and Ki-*ras* activation in lung tumors from resistant and susceptible mouse strains. *Mol Carcinog* 8: 177–185, 1993.
9. **Domej W, Földes-Papp Z, Schlagenhaufen C, Wippel R, Tilz GP, Krachler M, Demel U, Lang J, Urban-Woltron H.** Detection of graphite using laser microprobe mass analysis of a transbronchial biopsy from a foundry worker with mixed dust pneumoconiosis. *Wien Klin Wochenschr* 114: 216–221, 2002.
10. **Donaldson K, Aitken R, Tran L, Stone V, Duffin R, Forrest G, Alexander A.** Carbon nanotubes: a review of their properties in relation to pulmonary toxicology and workplace safety. *Toxicol Sci* 92: 5–22, 2006.
11. **Donaldson K, Tran L, Jimenez LA, Duffin R, Newby DE, Mills N, MacNee W, Stone V.** Combustion-derived nanoparticles: a review of their toxicology following inhalation exposure. *Part Fibre Toxicol* 2: 10–24, 2005.
12. **Dresselhaus MS, Dresselhaus G, Charlier JC, Hernández E.** Electronic, thermal and mechanical properties of carbon nanotubes. *Philos Transact A Math Phys Eng Sci* 362: 2065–2098, 2004.
13. **Driscoll KE, Costa DL, Hatch G, Henderson R, Oberdorster G, Salem H, Schlesinger RB.** Intratracheal instillation as an exposure technique for the evaluation of respiratory tract toxicity: uses and limitations. *Toxicol Sci* 55: 24–35, 2000.
14. **Dybdahl M, Risom L, Bornholdt J, Autrup H, Loft S, Wallin H.** Inflammatory and genotoxic effects of diesel particles in vitro and in vivo. *Mutat Res* 562: 119–131, 2004.
16. **Fadeel B, Kagan V, Krug H, Shvedova A, Svartengren M, Tran L, Wiklund L.** There's plenty of room at the forum: potential risks and safety assessment of engineered nanomaterials. *Nanotoxicology* 1: 73–84, 2007.
17. **Fiorito S, Serafino A, Andreola F, Togna A, Togna G.** Toxicity and biocompatibility of carbon nanoparticles. *J Nanosci Nanotechnol* 6: 591–599, 2006.
18. **Fraire AE, Greenberg SD.** Carcinoma and diffuse interstitial fibrosis of lung. *Cancer* 31: 1078–1086, 1973.
19. **Helland A, Wick P, Koehler A, Schmid K, Som C.** Reviewing the environmental and human health knowledge base of carbon nanotubes. *Environ Health Perspect* 115: 1125–1131, 2007.
20. **Hubbard R, Venn A, Lewis S, Britton J.** Lung cancer and cryptogenic fibrosing alveolitis. A population-based cohort study. *Am J Respir Crit Care Med* 161: 5–8, 2000.
21. **Huzcko A, Lange H, Calko E, Grubek-Jaworska H, Droszcz P.** Physiological testing of carbon nanotubes: are they asbestos-like? *Fullerene Sci Technol* 9: 251–254, 1997.
22. **Jackson MA, Lea I, Rashid A, Peddada SD, Dunnick JK.** Genetic alterations in cancer knowledge system: analysis of gene mutations in mouse and human liver and lung tumors. *Toxicol Sci* 90: 400–418, 2006.
23. **Junqueira LC, Bignolas G, Brentani RR.** Picrosirius staining plus polarization microscopy, a specific method for collagen detection in tissue sections. *Histochem J* 11: 447–455, 1979.
24. **Kasparov AA, Popova TB, Lebedeva NV, Gladkova EV, Gurvich EB.** Evaluation of the carcinogenic hazard in the manufacture of graphite articles. *Vopr Onkol* 35: 445–450, 1989.
25. **Khosravi-Far R, Der CJ.** The *ras* signal transduction pathway. *Cancer and Metastasis Reviews* 13: 67–89, 1994.
26. **Kipen HM, Laskin DL.** Smaller is not always better: nanotechnology yields nanotoxicology. *Am J Physiol Lung Cell Mol Physiol* 289: L696–L697, 2005.
27. **Knaapen AM, Borm PJ, Albrecht C, Schins RP.** Inhaled particles and lung cancer. Part A: mechanisms. *Int J Cancer* 109: 799–809, 2004.
28. **Lam CW, James JT, McCluskey R, Hunter RL.** Pulmonary toxicity of carbon nanotubes in mice 7 and 90 days after intratracheal instillation. *Toxicol Sci* 77: 126–134, 2004.
29. **Lam CW, James JT, McCluskey R, Arepalli S, Hunter RL.** A review of carbon nanotube toxicity and assessment of potential occupational and environmental health risks. *Crit Rev Toxicol* 36: 189–217, 2006.
30. **Li JG, Li WX, Xu JY, Cai XQ, Liu RL, Li YJ, Zhao QF, Li QN.** Comparative study of pathological lesions induced by multiwalled carbon

nanotubes in lungs of mice by intratracheal instillation and inhalation. *Environ Toxicol* 22: 415–421, 2007.
31. **Li XY, Brown D, Smith S, MacNee W, Donaldson K.** Short-term inflammatory responses following intratracheal instillation of fine and ultrafine carbon black in rats. *Inhal Toxicol* 11: 709–731, 1999.
32. **Li Z, Hulderman T, Salmen R, Chapman R, Leonard SS, Young SH, Shvedova AA, Luster MI, Simeonova PP.** Cardiovascular effects of pulmonary exposure to single-wall carbon nanotubes. *Environ Health Perspect* 115: 377–382, 2007.
33. **Maynard AD, Baron PA, Foley M, Shvedova AA, Kisin ER, Castranova V.** Exposure to carbon nanotube material: aerosol release during the handling of unrefined single walled carbon nanotube material. *J Toxicol Environ Health* 67: 87–107, 2004.
34. **Medina C, Santos-Martinez MJ, Radomski A, Corrigan OI, Radomski MW.** Nanoparticles: pharmacological and toxicological significance. *Br J Pharmacol* 150: 552–558, 2007.
35. **Mercer RR, Russell ML, Crapo JD.** Alveolar septal structure in different species. *J Appl Physiol* 77: 1060–1066, 1994.
36. **Mercer RR, Scabilloni J, Wang L, Kisin E, Murray AR, Schwegler-Berry D, Shvedova AA, Castranova V.** Alteration of deposition pattern and pulmonary response as a result of improved dispersion of aspirated single-walled carbon nanotubes in a mouse model. *Am J Physiol Lung Cell Mol Physiol* 294: L87–L97, 2008.
37. **National Institute for Occupational Safety and Health.** *Criteria for a Recommended Standard. Occupational Exposure to carbon Black. U. S. Department of Health, Education, and Welfare.* Rockville, MD: Centers for Disease Control, National Institute for Occupational Safety and Health, 1978.
38. **Nikula KJ, Snipes MB, Barr EB, Griffith WC, Henderson RF, Mauderly JL.** Comparative pulmonary toxicities and carcinogenicities of chronically inhaled diesel exhaust and carbon black in F344 rats. *Fundam Appl Toxicol* 25: 80–94, 1995.
39. **Oberdorster G, Ferin J, Lehnert E.** Correlation between particle size, in vivo particle persistence, and lung injury. *Environ Health Perspect* 102: 173–179, 1994.
40. **Oberdorster G.** Significance of particle parameters in the evaluation of exposure-dose-response relationships of inhaled particles. *Inhal Toxicol* 8: 73–89, 1996.
41. **Piguet PF, Collart MA, Grau GE, Sappino AP, Vassalli P.** Requirement of tumour necrosis factor for development of silica-induced pulmonary fibrosis. *Nature* 344: 245–247, 1990.
42. **Raabe OG, Al-Bayati MA, Teague SV, Rasolt A.** Regional deposition of inhaled monodisderse coarse and fine aerosol particles in small laboratory animals. *Ann Occup Hyg* 32: 53–63, 1988.
43. **Rao GV, Tinkle S, Weissman DN, Antonini JM, Kashon ML, Salmen R, Battelli LA, Willard PA, Hoover MD, Hubbs AF.** Efficacy of a technique for exposing the mouse lung to particles aspirated from the pharynx. *J Toxicol Environ Health* 66: 1441–1452, 2003.
44. **Roco MC.** Science and technology integration for increased human potential and societal outcomes. *Ann N Y Acad Sci* 1013: 1–16, 2004.
45. **Ronai ZA, Gradia S, Peterson LA, Hecht SS.** G to A transitions and G to T transversions in codon 12 of the Ki-*ras* oncogene isolated from mouse lung tumors induced by 4-(methylnitrosamino)-1-(3-pyridyl)-1-butanone (NNK) and related DNA methylating and pyridyloxobutylating agents. *Carcinogenesis* 14: 2419–2422, 1993.
45a. **Short SR, Petsonk EL.** Respiratory system: the variety of pneumoconioses. In: *Encyclopaedia of Occupational Health and Safety* (4th ed.), edited by Stellman JM. Geneva: International Labour Organization, 1998.
46. **Shvedova AA, Kisin ER, Murray AR, Schwegler-Berry D, Gandelsman VZ, Baron P, Maynard A, Gunther MR, Castranova V.** Exposure of human bronchial epithelial cells to carbon nanotubes causes oxidative stress and cytotoxicity. In: *Proc Soc Free Rad Research Meeting, European Section, June 26–29, 2003, Ioannina, Greece*, p. 91–103, 2004.
47. **Shvedova AA, Kisin ER, Mercer R, Murray AR, Johnson VJ, Potapovich AI, Tyurina YY, Gorelik O, Arepalli S, Schwegler-Berry D, Hubbs AF, Antonini J, Evans DE, Ku BK, Ramsey D, Maynard A, Kagan VE, Castranova V, Baron P.** Unusual inflammatory and fibrogenic pulmonary responses to single walled carbon nanotubes in mice. *Am J Physiol Lung Cell Mol Physiol* 289: L698–L708, 2005.
48. **Shvedova AA, Fabisiak JP, Kisin ER, Murray AR, Roberts JR, Tyurina YY, Antonini JM, Feng WH, Kommineni C, Reynolds J, Barchowsky A, Castranova V, Kagan VE.** Sequential exposure to carbon nanotubes and bacteria enhances pulmonary inflammation and infectivity. *Am J Respir Cell Mol Biol* 38: 579–590, 2008.
49. **Small JV.** Measurements of section thickness. In: *Proceedings of the 4th European Congress on Electron Microscopy*, edited by Bocciarelli D. S. 1968, p. 609–610.
50. **Stabile LP, Rothstein ME, Keohavong P, Jin J, Yin J, Land SR, Dacic S, Luong TM, Kim KJ, Dulak AM, Siegfried JM.** Therapeutic targeting of human hepatocyte growth factor with a single neutralizing monoclonal antibody reduces lung tumorigenesis. *Mol Cancer Ther* 7: 1913–1922, 2008.
52. **Tao F, Gonzalez-Flecha B, Kobzik L.** Reactive oxygen species in pulmonary inflammation by ambient particulates. *Free Radic Biol Med* 35: 327–340, 2003.
53. **U.S. Environmental Protection Agency.** *40 CFR Part 50: National Ambient Air Quality Standards for Ozone and Particulate Matter*. Final Rule 71, no. 200, 2006.
54. **Underwood EE.** Quantatative Stereology. Reading, MA: Addison-Wesley, 1970.
55. **Warheit DB, Laurence BR, Reed KL, Roach DH, Reynolds GA, Webb TR.** Comparative pulmonary toxicity assessment of single-wall carbon nanotubes in rats. *Toxicol Sci* 77: 117–125, 2004.
56. **Young IS, Trimble ER.** Measurement of malondialdehyde in plasma by high performance liquid chromatography with fluorimetric detection. *Ann Clin Biochem* 28: 504–508, 1991.